Compatibilizing Effect of Styrene–Maleic Anhydride Copolymer on the Properties of Polyamide-6/Liquid Crystalline Copolyester Composites

S. C. TJONG, R. K. Y. LI, X. L. XIE*

Department of Physics and Materials Science, City University of Hong Kong, Tat Chee Avenue, Kowloon, Hong Kong

Received 26 August 1999; accepted 19 October 1999

ABSTRACT: Liquid crystalline polymer–polyamide-6 (LCP/PA6) composites containing 20 wt % LCP content were compatibilized by a random styrene–maleic anhydride copolymer (RSMA). The blending was performed via extrusion followed by injection molding. The LCP employed was a commercial copolyester, Vectra A950. The dynamic mechanical (DMA), rheological, thermal, and mechanical properties as well as the morphology of the composites were studied. The DMA and rheological results showed that RSMA is an effective compatibilizer for LCP/PA6 blends. The mechanical measurements showed that the stiffness, tensile strength, and toughness of the *in situ* composites are generally improved with increasing RSMA content. However, these mechanical properties deteriorated considerably when RSMA content was above 10 wt %. The drop-weight dart impact test was also applied to analyze the toughening behavior of these composites. The results show that the maximum impact force (F_{max}) and crack-initiation energy (E_{init}) tend to increase with increasing RSMA content. From these results, it appeared that RSMA prolongs the crack-initiation time and increases the energies for crack initiation and impact fracture, thereby leading to toughening of LCP/PA6 *in situ* composites. Finally, the correlation between the mechanical properties and morphology of the blends is discussed. © 2000 John Wiley & Sons, Inc. J Appl Polym Sci 77: 1964–1974, 2000

Key words: polyamide-6; liquid crystalline copolyester; random styrene–maleic anhydride copolymer; compatibilization

INTRODUCTION

Blending of conventional thermoplastic polymers with liquid crystalline polymers (LCPs) has attracted considerable attention.[1–8] This is because LCPs can be deformed into fine and elongated fibrils within an isotropic matrix under appropriate processing conditions, leading to so-called *in situ* polymer composites. However, immiscibility and poor interfacial adhesion between the LCP dispersed phase and the thermoplastic matrix generally result in the LCP/thermoplastic blends having low tensile strength and impact toughness, so the development of *in situ* composites is restricted. A number of attempts have been made by polymer scientists to improve the miscibility and the interfacial adhesion between these two distinct phases. One widely used effective method involves the addition of a suitable compatibilizer. A compatibilizer is a copolymer consisting of two blocks that are similar to the polymer components

Correspondence to: S. C. Tjong.
* On leave from the Department of Chemistry, Huazhong University of Science and Technology, Wuhan, China
Contract grant sponsor: City University of Hong Kong; contract grant number: 7000607.
Journal of Applied Polymer Science, Vol. 77, 1964–1974 (2000)

in the blends or a functionalized polymer which undergoes chemical and/or physical reaction with dissimilar components of the blends. For example, Baird and coworkers[4,9–11] as well as Tjong and Meng[7,12–14] reported that maleic anhydride-grafted polypropylene (MAP) is an effective compatibilizer for improving the mechanical properties of LCP/polypropylene (PP) and LCP/polyamide-6 blends. Weiss and coworkers[15,16] indicated that a metal salt containing slightly sulfonated polystyrene ionomers can be used to compatibilize LCP/ polyamide blends. Miller et al.[17] employed an acrylic acid-functionalized PP to compatibilize LCP/PP polyblend fibers. Recently, Holsti-Miettinen et al.[18] pointed out that an epoxy-functionalized polymer addition significantly improves the impact strength of LCP/PP blends.

Polyamide-6 (PA6) is a semicrystalline polymer and used extensively in the manufacture of automobile parts, engineering structures, and textile fibers owing to its high mechanical strength, stiffness, and good processability. However, PA6 exhibits a low heat-deflection temperature (HDT), low crack propagation resistance, and high moisture absorption, which limit its usage as a structural component for industrial applications. These shortcomings can be overcome by blending PA6 with LCPs. The morphology and mechanical properties of molecular composites and *in situ* composites based on the polyamide (PA) and LCPs were investigated by various workers.[7,19–27] The LCPs used by them include wholly aromatic PAs (such as PBA, PPTA, and PPD-T), copolyester (such as Vectra A950), and copolyesteramide (such as Vectra B950). Their results indicated that LCP addition leads to an increase in both the tensile strength and the modulus of the blends, but to a decrease in the elongation at break owing to poor interfacial adhesion. As mentioned above, the addition of a compatibilizer is an effective route to enhance the adhesion between the LCP and the PA matrix. According to the literature,[28] the random styrene–maleic anhydride copolymer (RSMA) shows excellent processability, high heat resistance, HDT, and stiffness at high temperature. Its processing temperature is over 300°C. Because RSMA contains about 5–33mol % of MA, it is an excellent modification agent and compatibilizer for thermoplastics and polymer alloys.[2] Little information is available in the literature concerning the compatibilizing of RSMA on the thermal and mechanical properties of LCP/PA composites. In the present work, we attempted to blend PA6 with a 20 wt % Vectra A950 liquid crystalline copolyester in the present of RSMA as a compatibilizer.

EXPERIMENTAL

Materials

The LCP used in this work is commercial Vectra A950 from Ticona Co. (USA) based on 2,6-hydroxynaphthoic acid and *p*-hydroxybenzoic acid. PA6 pellets (Novamid) produced by Mitsubishi Engineering-Plastics Corp. (Taiwan) were used as the matrix material. RSMA (MA 12 mol %) was supplied by the Shanghai Gaoqiao Petro-Chemical Co. (Shanghai, China). The LCP, RSMA, and PA6 pellets were dried in an oven at 120°C for 48 h before mixing.

Sample Preparation

LCP/PA6 blends containing 20 wt % LCP were prepared in a twin-screw Brabender Plasticorder at 290°C and 50 rpm. The resulting blends were then mixed with 0, 2.5, 5, 10, and 15 wt % RSMA under the above conditions. The extrudates exiting from the Brabender were cut into pellets by a pelletizer. The plaques with dimensions of 200 $\times$ 80 $\times$ 3.2 mm^3 were injection-molded from these pellets. The barrel-zone temperatures of the injection molder were set at 280, 285, and 285°C. The extrusion and injection temperatures of the LCP/PA6 blends were kept at 285–290°C because PA6 tends to decompose thermally at temperatures above 300°C during the blending of LCP/PA6 blends. Consequently, LCP fibrillation did not take place in the injection-molded LCP/PA6 blend specimens processed at temperatures above 300°C.[12] In a previous study, Meng and Tjong observed that LCP fibrils are developed in the skin section of MA-compatibilized LCP/PA6 blends. Such composites were injection-molded at 285°C.[13]

The injection-molded plaques were cut into dog-bone-shaped tensile bars. Notched Izod impact specimens were also prepared from the plaques. Both longitudinal and transverse specimens were used for the tensile and impact tests. For the longitudinal specimens, the length direction was parallel to the flow direction, while it was perpendicular to the flow direction for the transverse specimens.

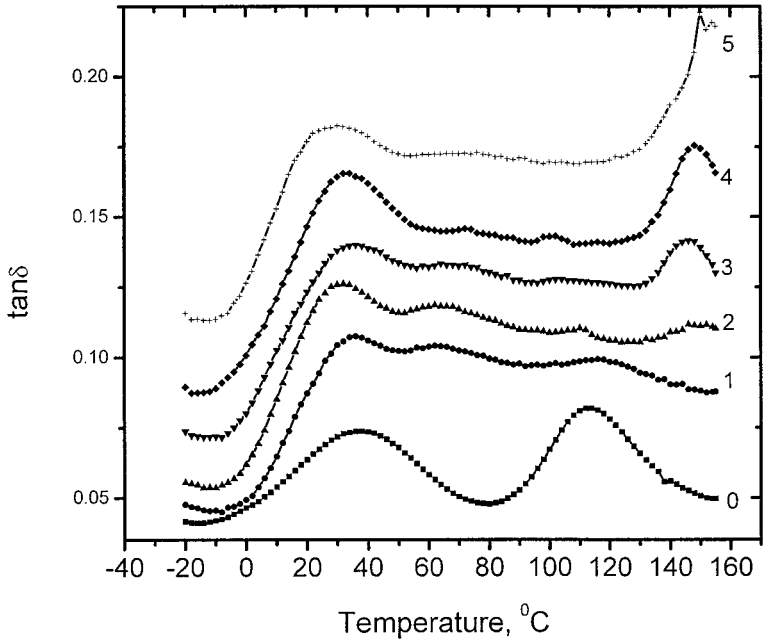

Figure 1 Variation of the loss modulus with temperature for LCP and LCP/PA6 blends: (0) LCP; (1) LCP/PA6 20/80; (2) LCP/PA6/RSMA 19.5/78/2.5; (3) LCP/PA6/RSMA 19/76/5; (4) LCP/PA6/RSMA 18/72/10; (5) LCP/PA6/RSMA 17/68/15.

Dynamic Mechanical Analysis (DMA)

DMA was conducted with a DuPont dynamic mechanical analyzer (Model 983) at a fixed frequency of 1 Hz and an oscillation amplitude of 0.15 mm. The samples with dimensions of 50 × 15 × 3.2 mm^3 were prepared from injection molded plates. The temperature range studied was from −10 to 170°C with a heating rate of 2°C min^{-1}.

FTIR Spectra

Fourier transform infrared spectroscopy (FTIR) was applied to characterize the changes in the chemical structure of LCP/PA6 blends after RSMA addition. Thin-film specimens were prepared using a Reichert-Jung Sliding Microtome System (Cambridge Instruments GambH). The tests were conducted with a Perkin–Elmer 16 PC spectrophotometer.

Torque Measurements

The melting torques of the pure PA6, LCP, RSMA, and their blends were determined with a Brabender Plasticorder at a capacity of 50 cm^3 and operated at 285°C and 75 rpm for 10 min.

Differential Scanning Calorimetry (DSC)

DSC measurements were conducted with a Perkin–Elmer DSC-7 instrument at a heating rate of 10°C min^{-1} under a dry nitrogen atmosphere. Prior to the DSC recording, all samples were heated to 300°C and kept at this temperature for 3 min to eliminate the influence of their previous thermal histories. They were then quenched to ambient temperature. For nonisothermal crystallization measurement, the samples were heated to and kept at 300°C for 3 min, then cooled at a cooling rate of 10°C min^{-1}.

Mechanical Properties

Tensile behavior was determined using an Instron tester (Model 4206) at room temperature under a crosshead speed of 1 mm min^{-1}. Izod impact specimens with dimensions of 65 × 13 × 3.2 mm^3 were cut from the plaques and tested by a Ceast impact pendulum tester. These speci-

Table I Glass Transition Temperatures of LCP/PA6/RSMA Blends

LCP/PA6/RSMA	T_{g1} (°C)	T_{g2} (°C)
20/80/0	61.7	118.0
19.5/78/2.5	65.2	110.5
19/76/5	69.1	105.0
18/72/10	73.3	102.3
17/68/15	75.6	101.2

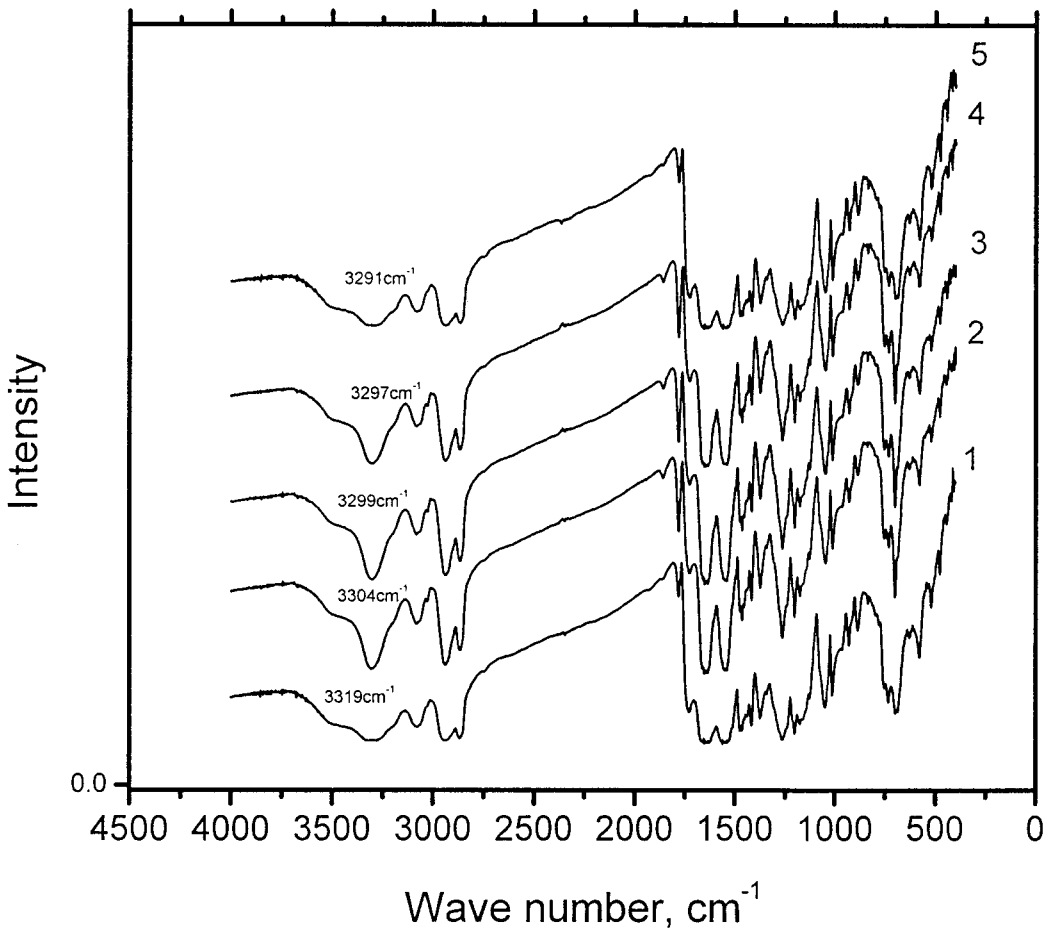

Figure 2 FTIR spectra of (1) LCP/PA6 20/80, (2) LCP/PA6/RSMA 19.5/78/2.5, (3) LCP/PA6/RSMA 19/76/5, (4) LCP/PA6/RSMA 18/72/10, and (5) LCP/PA6/RSMA 17/68/15.

mens were sharply notched with a Ceast cutter with a notch tip radius of 0.25 mm. For the instrumented drop-weight dart impact tests, the injection-molded plaques were cut into equal halves, each having dimensions of $100 \times 80 \times 3.2$ mm^3. A total of five samples were tested for each blend. A Ceast Fractovis instrumented drop-weight impact tester with a hemispherical tip (tip diameter = 20 mm) was used for the tests. The samples were fully clamped by an annular support ring and a movable clamp mechanism. The exposed surface for impact was circular in shape with a diameter of 38.1 mm. The impact velocity was 2 m s^{-1}.

Morphology Observations

The morphologies of the fracture surfaces were observed in a scanning electron microscope (SEM, Model JEOL JSM 820). The specimens were cut from the injection-molded plaques along the flow direction. They were fractured in liquid nitrogen. All fractured surfaces were coated with a thin layer of gold prior to SEM examination.

RESULTS AND DISCUSSION

Dynamic Mechanical Properties

Figure 1 shows the loss factor (tan δ) versus temperature for the specimens investigated. The glass transition temperatures (T_g's) of PA6 and LCP/PA6 blends determined from the loss factor are listed in Table I. The T_g of PA6 and LCP are located at about 61.7 and 118.0°C, respectively. The peak located at 35.0°C is associated with the β-transition of the LCP. From Table I, it can be

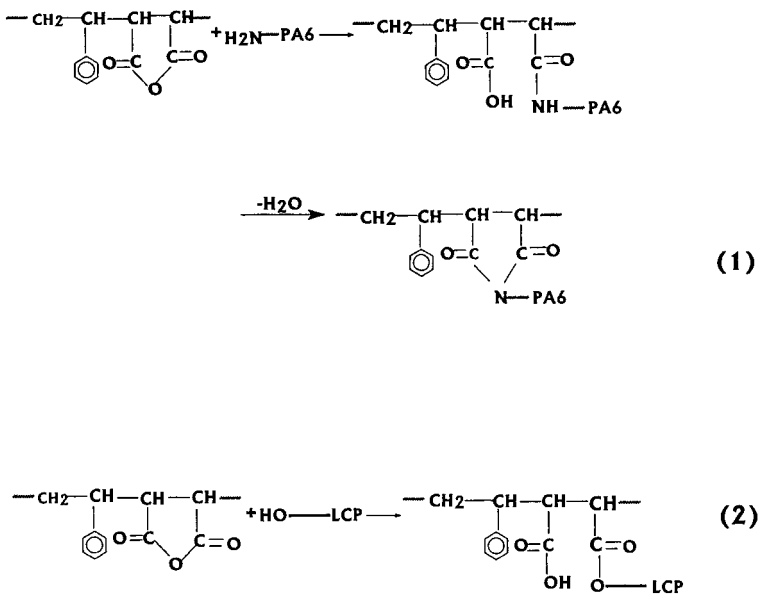

Figure 3 Schematic diagram showing the reactions between functional groups of RSMA and PA6 and between RSMA and LCP.

seen that the LCP/PA6 blends show two glass transitions, indicating that the blends are heterogeneous, that is, consist of PA6 and LCP phases. However, the two peaks shift toward each other with increasing RSMA concentration. Thus, the compatibility between the LCP and PA6 phases is improved accordingly. These results indicate that RSMA can compatibilize the blend components of LCP/ PA6 specimens effectively.

FTIR Spectra

Figure 2 shows the FTIR spectra of LCP/PA6 blends containing various RSMA contents. The wide absorption peak located at about 3319 cm^{-1} is associated with the stretching vibration of the amino groups of PA6 and the hydroxyl end-groups of LCP. By adding 2.5 wt % of RSMA in the LCP/PA6 blend, such an absorption band shifts to 3304 cm^{-1}. With increasing RSMA content in the LCP/PA6 blends, this absorption band shifts to a lower wavenumber. This may be due to the formation of hydrogen bonding and/or an amide reaction between RSMA and PA6 and to the formation of hydrogen-bonding and/or an esterification reaction between RSMA and the LCP as shown in Figure 3.

Torque Behavior

Figure 4 shows the typical torque curves for LCP/PA6 20/80 and LCP/PA6/RSMA 19.5/78/2.5 blends mixed at 285^{0}C. It can be seen that these torque curves show an apparent maximum, and they then gradually approach a steady-state value after 10 min. The apparent maximum in torque curves is caused by the initial loading of the solid pellets; thus, we only analyzed the steady-state torque values associated with the flow of the molten pellets. Table II lists the steady torque values of pure PA6, LCP, RSMA, and their

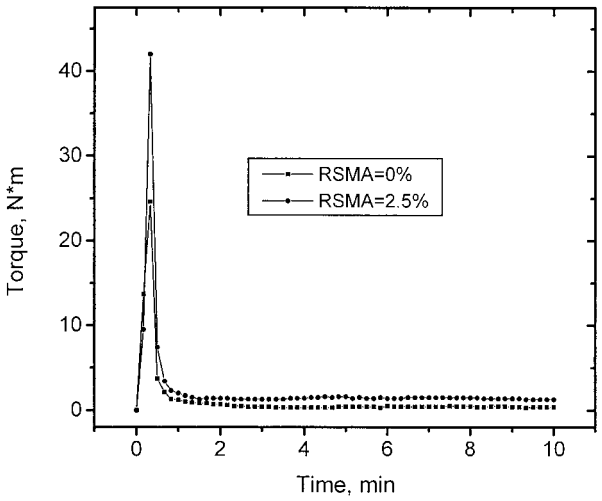

Figure 4 Torque curves of LCP/PA6 20/80 and LCP/PA6/RSMA 19.5/78/2.5 blends.

Table II Steady Torque Values of LCP/PA6/RSMA Blends

LCP/PA6/RSMA	Torque (N m)
100/0/0	2.4
0/100/0	0.6
0/0/100	2.4
20/80/0	0.4
19.5/78/2.5	1.3
19/76/5	1.1
18/72/10	1.1
17/68/15	1.2

blends at 10 min. The typical deviation or uncertainty for the steady torque values is about ±5%. From Table II, the steady torque value of PA6 is 0.6, while the value of LCP/PA6 20/80 is 0.4 N m. Apparently, the melt torque of the PA6 is reduced by adding 20 wt % LCP. This is because the LCP acts as a processing aid to PA6, thereby reducing the melt viscosity of the PA6 matrix. However, the steady torques of the LCP/PA6 blends appear to increase with the incorporation of RSMA. This is because RSMA enhances the intermolecular interactions between the LCP and PA6 as discussed above.

Thermal Properties

Figures 5 and 6 show DSC heating and cooling thermograms for PA6 and LCP/PA6 blends. The melting (T_m), crystallization temperature (T_c), and heat of fusion (ΔH_m) of these samples are determined from these curves. The degree of crystallinity (X_c) of LCP/PA6 blends can be determined from their heat of fusion normalized to that of PA6. The heat of fusion of 100% crystalline PA6 is estimated to be 193.81 J/g according to the literature.[30] The results are listed in Table III. Apparently, T_m, T_c, and ΔH_m of the PA6 phase in LCP/PA6/RSMA blends almost remain unchanged with increasing RSMA concentration. This indicates that the addition of RSMA does not affect the melting and crystallizing behaviors, possibly because RSMA only enhances the compatibility between the LCP and PA6 in the LCP/PA6/RSMA blends.

Mechanical Properties

The variation of the Young's modulus and tensile strength with RSMA content for ternary LCP/PA6/RSMA samples in both longitudinal and transverse directions is shown in Figures 7 and 8. Apparently, the Young's modulus and tensile strength of the longitudinal blends are much higher than are those of the transverse samples. This is typical behavior of the composites rein-

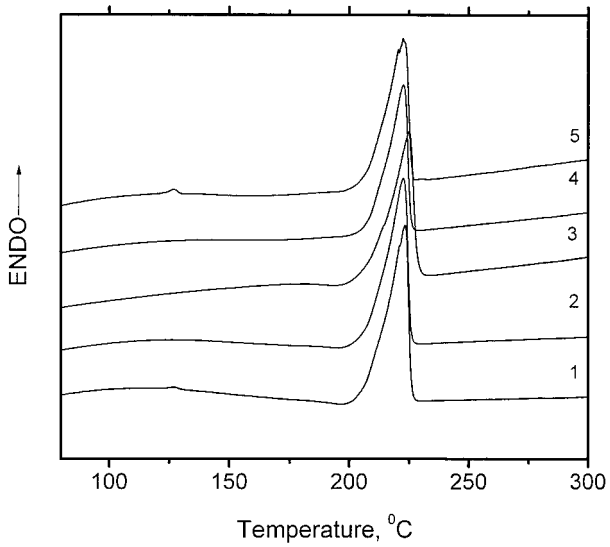

Figure 5 DSC heating scanning curves of (1) LCP/PA6 20/80, (2) LCP/PA6/RSMA 19.5/78/2.5, (3) LCP/PA6/RSMA 19/76/5, (4) LCP/PA6/RSMA 18/72/10, and (5) LCP/PA6/RSMA 17/68/15.

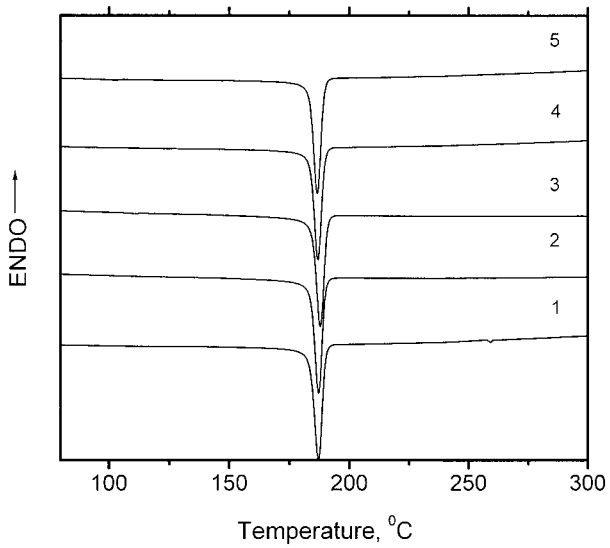

Figure 6 DSC cooling curves of (1) LCP/PA6 20/80, (2) LCP/PA6/RSMA 19.5/78/2.5, (3) LCP/PA6/RSMA 19/76/5, (4) LCP/PA6/RSMA 18/72/10, and (5) LCP/PA6/RSMA 17/68/15.

Table III Thermal Properties of LCP/PA6/RSMA Blends

LCP/PA6/RSMA	T_m (°C)	ΔH_m [a] (J/g)	T_c (°C)	X_c (%)
20/80/0	210.5	73.78	191.0	38.1
19.5/78/2.5	210.2	70.54	190.2	36.4
19/76/5	211.5	70.26	190.3	36.3
18/72/10	211.0	69.87	190.0	36.1
17/68/15	210.7	69.63	189.7	35.9

[a] Corrected for per gram of PA6 in the blends.

forced with short fibers. As LCP fibrils are formed in the LCP/PA6/RSMA samples as discussed in the next section, it is likely that their mechanical performance is similar to that of short-fiber-reinforced composites. It can also be seen from these figures that the addition of only 5–10 wt % RSMA to the binary LCP/PA6 blend results in an obvious increase in both the Young's modulus and the tensile strength of the longitudinal and transverse samples. When the RSMA content is >10 wt %, the stiffness and tensile strength of the longitudinal and transverse samples tend to decrease slowly with increasing RSMA content. Figure 9 shows the impact strength versus the RSMA content for both longitudinal and transverse specimens of LCP/PA6/RSMA blends. This figure indicates that the impact strengths of these composites increase with increasing RSMA content up to 10 wt %. Thereafter, they decrease with

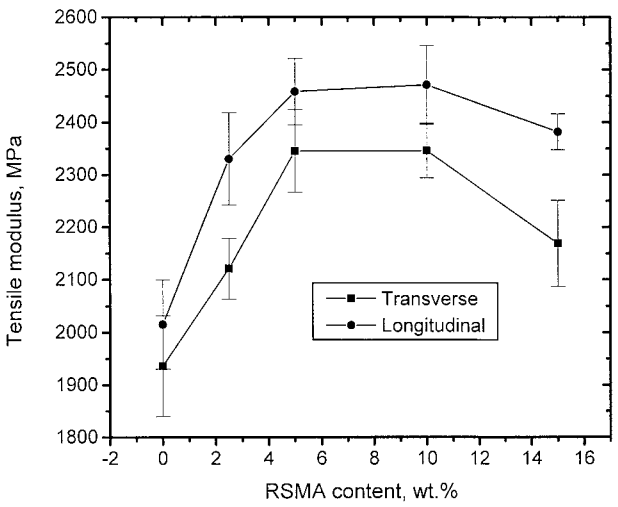

Figure 7 Young's modulus versus RSMA content for LCP/PA6 20/80 and ternary LCP/PA6/RSMA blends.

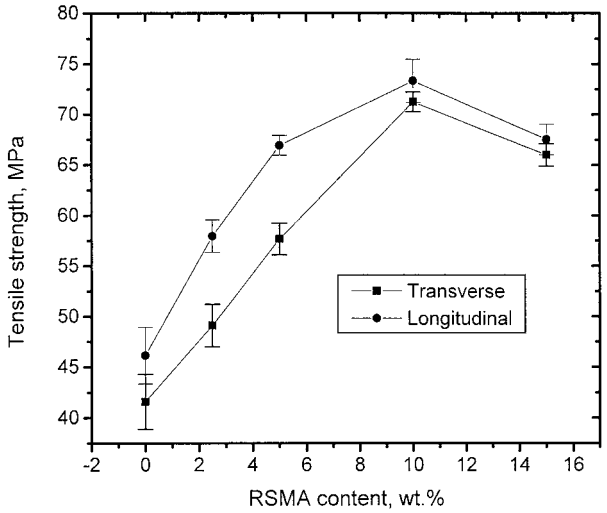

Figure 8 Tensile strength versus RSMA content for LCP/PA6 20/80 and ternary LCP/PA6/RSMA blends.

increasing RSMA content. From these results, it is clear that the addition of RSMA enhances the compatibility and interfacial adhesion between the LCP and PA6 phases, thereby greatly improving the mechanical stiffness, strength, and impact toughness of the LCP/PA6/RSMA composites. It is noted that the longitudinal impact strength of the LCP/PA6/RSMA blends are within 1.5–3.5 kJ/m^2, which means that these improvements reported are not significant for practical applications.

Finally, we used the drop-weight dart impact test to analyze the fracture process and to under-

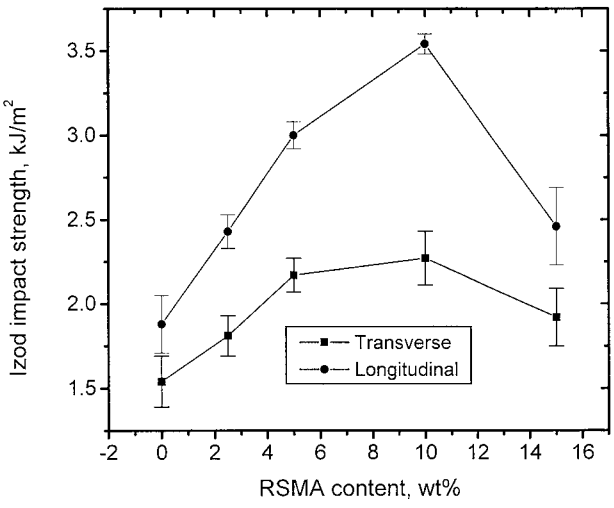

Figure 9 Izod impact strength versus RSMA content for LCP/PA6 20/80 and ternary LCP/PA6/RSMA blends.

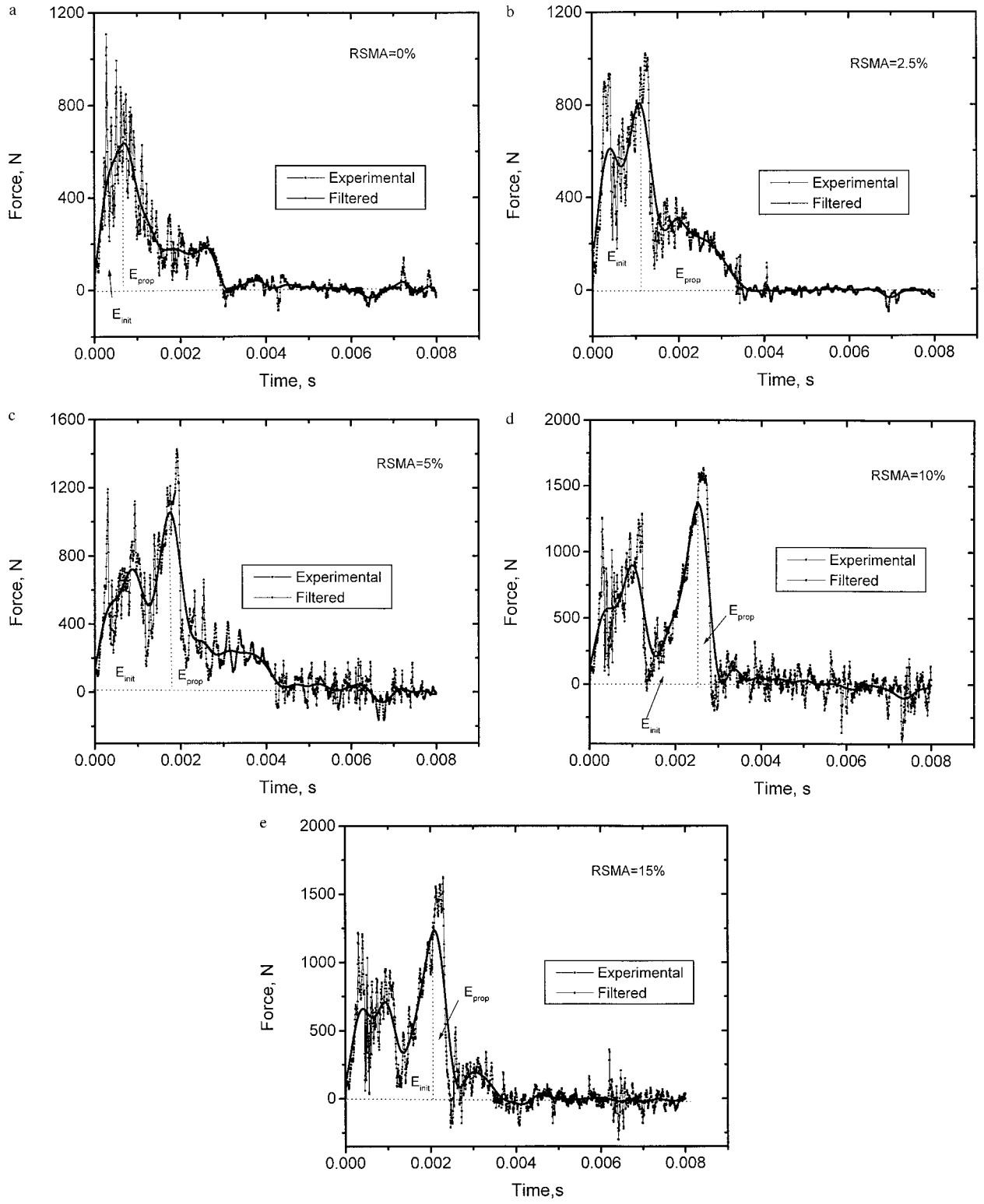

Figure 10 Force–time curves of the drop-weight dart impact test for the *in situ* composites.

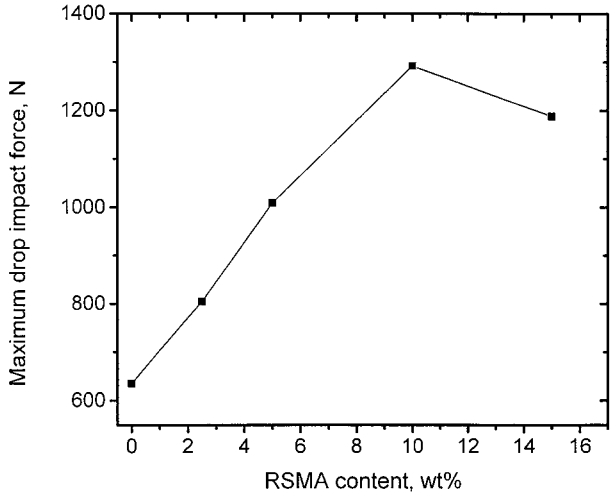

Figure 11 The F_{max} versus the RSMA content for the *in situ* composites.

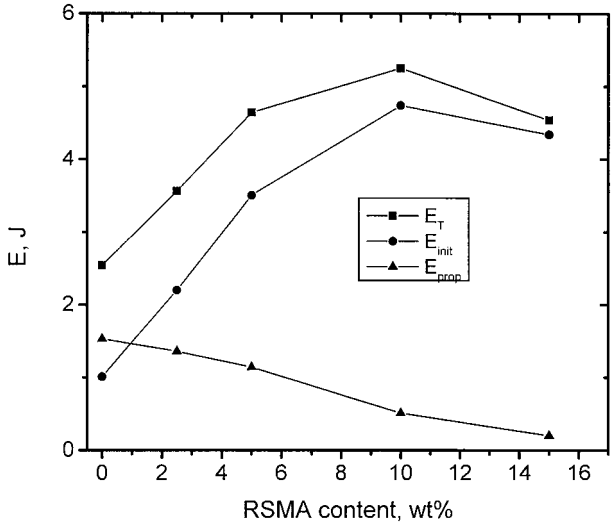

Figure 12 Drop-weight impact energies, E_{init}, E_{prop}, and ET versus the RSMA content.

stand the toughening mechanics more clearly. Figure 10(a–e) shows typical force–time curves for the *in situ* LCP/PA6 composites without and with RSMA. It can be seen that these curves exhibit various noises due to the force oscillations during the drop-weight test. Some workers applied electrical and mechanical filtering to treat the experimental signals.[31,32] In this work, we made use of Fourier transform to filter the noise from the experimental signals. The results are also shown in Figure 10(a–e). From Figure 10, five parameters can be easily identified: (a) the maximum force, F_{max}; (b) the energy absorbed up to the maximum force, which is defined as the initiation energy, E_{init}; (c) the propagation energy, E_{prop}; (d) the total fracture energy, E_T; and (e) the load rise time up to the force peak position, T_r. These parameters for *in situ* LCP/PA6 composites without and with RSMA are summarized in Figures 11–13. It is apparent that F_{max}, E_{init}, E_T, and T_r appear to increase with increasing RSMA content. When the RSMA content is above 10 wt %, these values tend to decrease. These behaviors are in accordance with the above tensile and Izod notched impact properties. It is noticed that E_{prop} decreases with increasing RSMA content. From these results, we believe that RSMA prolongs the crack-initiation time and increases the energies for crack initiation and impact fracture, leading, therefore, to toughening of LCP/PA6 *in situ* composites.

Morphology

Figure 14(a,b) shows low-magnification SEM fractographs of the LCP/PA6 20/80 and LCP/PA6/RSMA 19.5/78/2.5 composite specimens. Important information about the nature of a fracture can be obtained from microscopic examination of the fracture surface. This study is usually called fractography and is most commonly done using SEM.[33] From these figures, it can be seen that the binary LCP/PA6 blend containing 20 wt % LCP exhibits a typical skin–core structure. Such a

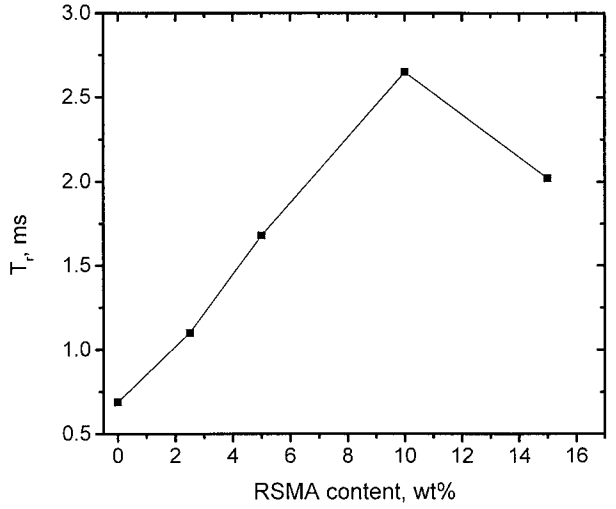

Figure 13 The load rise time up to the peak position (T_r) versus RSMA content for the *in situ* composites.

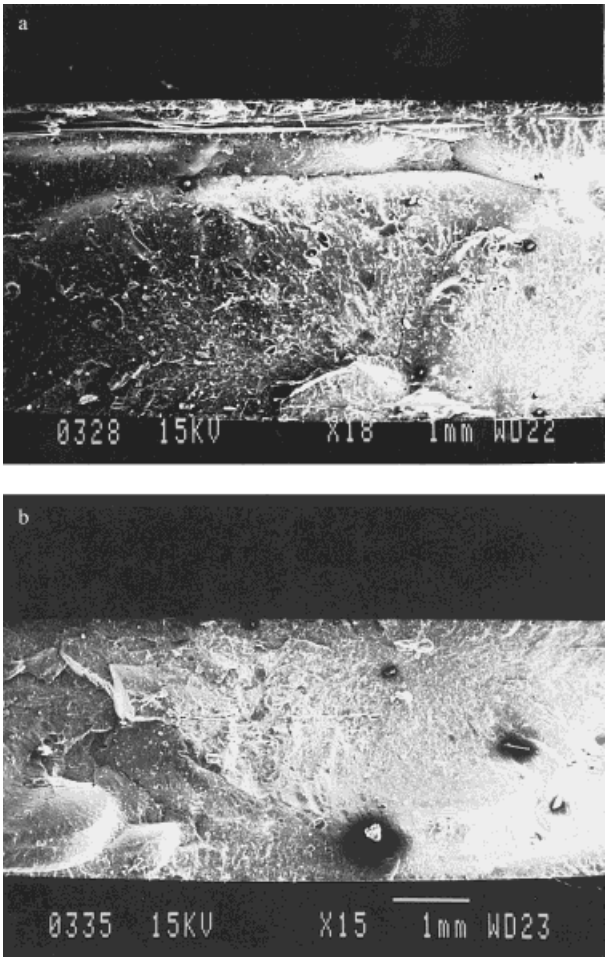

Figure 14 Low-magnification SEM fractographs of the injection-molded (a) LCP/PA6 20/80 and (b) LCP/PA6/RSMA 19.5/78/2.5 composites.

structure gradually disappears by adding 2.5 wt % RSMA. Figures 15 and 16 are higher-magnification views of the skin and core regions of LCP/PA6 20/80 and LCP/PA6/RSMA 19.5/78/2.5 composites. It is apparent that LCP fibrils are developed in the skin region of the LCP/PA6 20/80 composite. The adhesion between the fibrils and matrix is relatively poor as evidenced by the formation of the grooves in the fractograph associated with the pullout of fibers from the matrix [Fig. 15 (a)]. Furthermore, LCP droplets with a diameter of about 5–40 μm are observed in the core region of the composite. Cavities associated with the debonding of droplets from the matrix can be readily seen [Fig. 15 (b)]. On the other hand, fine LCP fibrils are developed in the skin section by adding 2.5 wt % RSMA in the LCP/PA6 blend [Fig. 16(a)]. The diameter of the LCP droplets appears to decrease (about 5–10 μm) in the core region. This indicates that RSMA improves the fibrillation and the dispersion of LCP in the PA6 matrix. These are related to the compatibilization effect of RSMA.

CONCLUSIONS

LCP/PA6 composites compatibilized by RSMA were prepared by injection molding. Their properties and morphology were systematically studied. The DMA, FTIR, and rheological results showed that RSMA was an effective compatibilizer for LCP/PA6 blends. The mechanical tests showed that the stiffness, tensile strength, and impact toughness of the *in situ* composites were

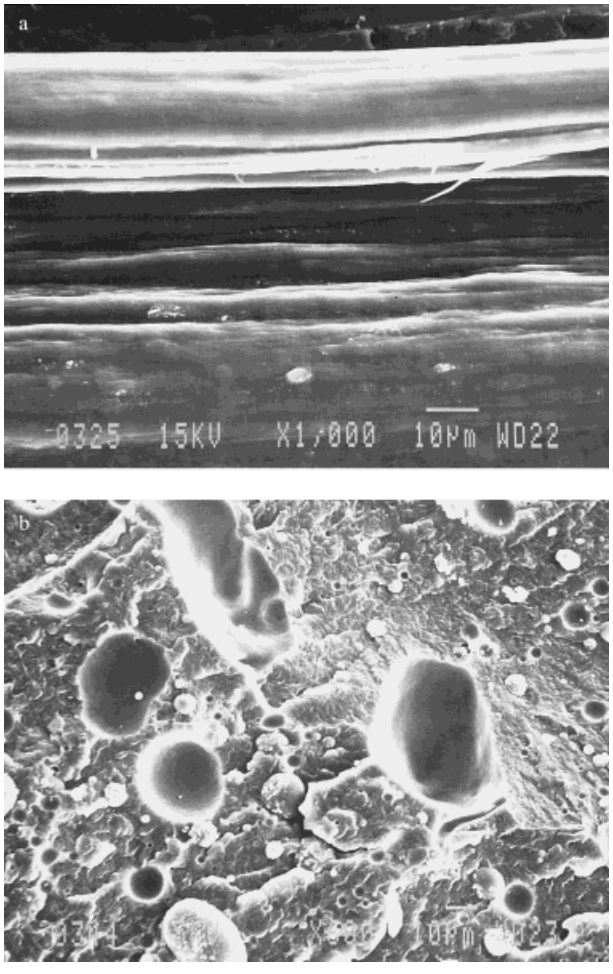

Figure 15 Higher-magnification SEM fractographs for (a) the skin and (b) core sections of injection-molded LCP/PA6 20/80 composite.

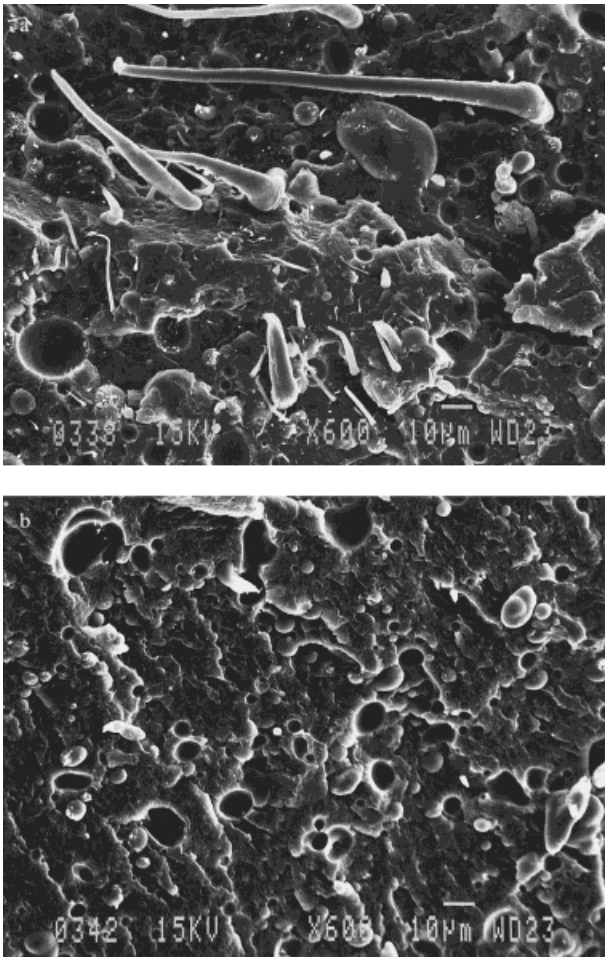

Figure 16 SEM fractographs of (a) the outer and (b) central sections of injection-molded LCP/PA6/RSMA 19.5/78/2.5 composites.

generally improved with increasing the RSMA content. When RSMA content was above 10 wt %, these mechanical properties deteriorated considerably. The drop-weight dart impact tester showed that F_{max}, E_{init}, E_T, and T_r also increased with increasing RSMA. But these values all tended to decrease when the RSMA content was above 10 wt %. From these results, we conclude that RSMA prolongs the crack-initiation time and increases the energies of crack initiation and impact fracture, thereby leading to toughening of LCP/PA6 *in situ* composites.

This work was supported by a Strategic Grant (No.7000607), City University of Hong Kong.

REFERENCES

1. Kiss, G. Polym Eng Sci 1987, 27, 410.
2. Done, D.; Baird D. G. Polymer 1990, 30, 989.
3. Limtasiri, T.; Isayev, A. I. J Appl Polym Sci 1991, 42, 2923.
4. Datta, A.; Baird, D. G. Polymer 1993, 34, 759.
5. Turek, D.; Simon, G. P. Polymer 1993, 34, 2750.
6. Tjong, S. C.; Liu, S. L.; Li, R. K. Y. J Mater Sci 1996, 31, 479.
7. Tjong, S. C.; Meng, Y. Z. Polymer 1997, 38,4609.
8. Tjong, S. C.; Chen, S. X.; Li, R. K. Y. J Appl Polym Sci 1997, 64, 705.
9. Bretas, R. E. S.; Baird, D. G. Polymer 1992, 33, 5233.
10. Datta, A.; Baird, D. G. Polymer 1995, 36, 505.
11. O'Donnell, H. T.; Baird, D. G. Polymer 1995, 36, 3113.
12. Tjong, S. C.; Meng, Y. Z. Polym Int 1997, 42, 209.
13. Meng, Y. Z.; Tjong, S. C. Polymer 1998, 39, 99.
14. Meng, Y. Z.; Tjong, S. C., Hay, A. S. Polymer 1998, 39, 1845.
15. Sullivan, M. J.; Weiss, R. A. Polym Eng Sci 1992, 32, 517.
16. Datta, D.; Weiss, R. A.; He, J. Polymer 1996, 37, 429.
17. Miller, M. M.; Cowie, J. M.; Tait, J. G.; Brydon, D. L.; Mather, R. R. G. Polym Eng Sci 1995, 36, 3107.
18. Holsti-Miettinen, R. M.; Heino, M. T.; Seppala, J. V. J. Appl Polym Sci 1995, 57, 573.
19. Carpaneto, L.; Lesage, G.; Pisino, R.; Trefiletti, V. Polymer 1999, 40, 1781.
20. Takayanagi, M.; Ogata, T.; Morikawa, M.; Kai, T. J Macromol Sci Phys B 1980, 17, 591.
21. Weiss, R, A.; Huh, W.; Nicolais, L. Polym Eng Sci 1987, 27, 684.
22. Blizard, K. G.; Baird, D. G. Polym Eng Sci 1987, 27, 653.
23. Beery, D.; Kenig, S.; Siegmann, A. Polym Eng Sci 1991, 31, 451.
24. Jang, S. H.; Kim, B. S. Polym Eng Sci 1994, 34, 847.
25. Yongsok, S. J Appl Polym Sci 1997, 64, 359.
26. La Mantia, F. P.; Valenza, A.; Paci, M.; Magagnini, P. L. J Appl Polym Sci 1989, 38, 583.
27. La Mantia, F. P.; Valenza, A.; Paci, M.; Magagnini, P. L. Polym Eng Sci 1990, 30, 7.
28. Culbertson, B. M. In Encyclopedia of Polymer Science and Engineering; Wiley: New York, 1987.
29. Utracki, L. A. Commercial Polymer Blends; Chapman & Hall: London, 1998.
30. Van Krevelen, D. W. Properties of Polymer, 3rd revised ed.; Elsevier: Amsterdam, 1997.
31. Mills, N. J.; Zhang, P. S. J Mater Sci 1989, 24, 2099.
32. Aggag, G.; Takahashi, K. Polym Eng Sci 1996, 36, 2260.
33. Dieter, G. E. Mechanical Metallurgy; McGraw-Hill: New York, 1988; p 254.